Investigating the Spot Weld Fatigue Crack Growth Process Using X-ray Imaging

An examination of the fatigue failure process of tensile-shear spot welded specimens took place, and the fatigue crack initiation location and propagation process were observed

BY G. WANG AND M. E. BARKEY

ABSTRACT. An x-ray technique was used to investigate the fatigue crack initiation and crack propagation processes of spot welded joints. The fatigue cracks usually initiate 0.2–1.0 mm from the nugget edge of the spot weld. Finite element and theoretical analyses indicated that the maximum stress concentration is away from the nugget root. Three different fatigue crack propagation modes have been observed that correspond to different loading amplitude regimes. Lastly, fatigue crack propagation rates are presented for galvannealed and galvanized metals.

Introduction

The fatigue crack growth behavior at a spot welded joint is important since it is often assumed to be a significant portion of the total fatigue life of the joint. Because of visual limitations of the crack initiation locations, as shown in Fig. 1, direct observation and measurement of fatigue crack growth during the cyclic loading are very difficult or expensive. An effective method to observe and understand the fatigue crack growth process is significant. Some techniques that have been previously applied have been based on sectioning multiple specimens or making indirect measurements that can be corroborated to crack growth. Alternatively, the failure process is often inferred from the final fracture surfaces of the joint.

Pollard (Ref. 1) studied the fatigue failure of spot welded joints and divided the failure modes into the following four types: interfacial failure, heat-affected zone (HAZ) failure, "ear" formed failure, and partial HAZ and base metal failure. Davidson et al. (Ref. 2) divided the fatigue failure as S (failure through the sheet), N (failure across the weld nugget), SN (shear failure of the nugget), and NS (failure across the weld nugget and sheet). Barkey et al. (Ref. 3) conducted the experimental study of the fatigue failure of combined loading spot welded specimens by using a special fixture to apply different ratios of shear and tensile load. Three types of failure modes have been described in the latter experiments — the sheet crack propagation mode, the sheet tearing mode, and the nugget pullout mode. Because of the lack of direct observation of the fatigue crack growth process, almost all of the modes of classification are based on the final broken forms of the specimens.

To expose the interior of the joint for observation during the crack growth process, McMahon et al. (Ref. 4) sectioned spot welded specimens and then applied fatigue loading, so that crack growth could be monitored visually. He found that approximately 50% of the total life was devoted to developing a 0.25-mm through-thickness crack under constant-amplitude loading in the life range of 10^4 to 10^6 cycles. This percentage appeared to increase at lives greater than 10^6 cycles. It is noted that the boundary or loading conditions by using a half-specimen are different from those of a typical joint during fatigue testing.

Cooper et al. (Ref. 5) developed a potential difference method to measure the fatigue crack growth of spot welded joints. In this method, electrodes are placed on the specimen, and a voltage change is observed as the fatigue cracks develop and grow near the spot weld. Alternatively, Barkey, Wang, and coworkers (Refs. 6, 7) have used natural frequency response measurements of the joint. The variation in these measurements was corroborated with finite element calculations and x-ray detection of the cracks. As a part of this study, a detailed investigation of crack growth behavior at the tensile-shear joint was conducted.

Another important characteristic of fatigue cracks in spot welded joints is the crack initiation location. Satoh et al. (Ref. 8) used a three-dimensional, elastic-plastic finite element method to analyze the tensile-shear spot welded specimen and found that the largest strain sometimes occurred at the position slightly away from the heat-affected zone in the base metal sheet. Similar to the fatigue failure mode, the crack initiation location is complex and usually involves many factors, such as the loading mode, material properties, nugget geometry, and others.

This paper presents an investigation and observations of the fatigue crack growth process of tensile-shear spot welded specimens. The x-ray image technique, employed previously (Ref. 6), is used to obtain the length and location of cracks developed during fatigue testing. The loading influence on the fatigue crack initiation location is examined first, and theoretical and finite element analyses are conducted to better understand the crack initiation location. Subsequently, the fatigue failure modes are classified according to the observed fatigue crack growth process, and both the fatigue crack growth with respect to the cyclic loading amplitude and fatigue life are also discussed.

KEYWORDS

Tensile-Shear Spot Weld
X-ray
Fatigue Crack
Crack Initiation
Crack Propagation
Stress Intensity Factor

Testing Method

Preparation of Tensile-Shear Spot Welded Specimens

The spot welded joints were produced using a Thompson 100-kVA A1 press-type spot welding machine. Copper electrodes with a 6.6-mm-diameter circular tip were used for all specimens. In order to ensure the quality of welding and prevent an irregular nugget geometry and excessive expulsion, a series of peel tests was con-

G. WANG and M. E. BARKEY (mbarkey@coe.eng.ua.edu) are with the Department of Aerospace Engineering and Mechanics, the University of Alabama, Tuscaloosa, Ala.

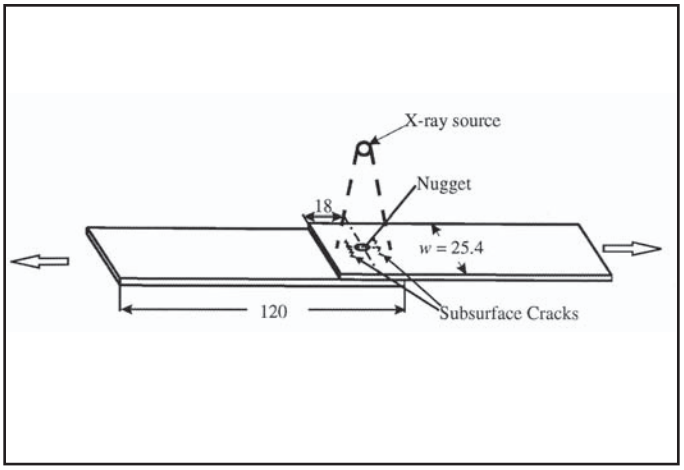

Fig. 1 — Test specimen shape, dimensions (mm), loading directions, and x-ray test setup.

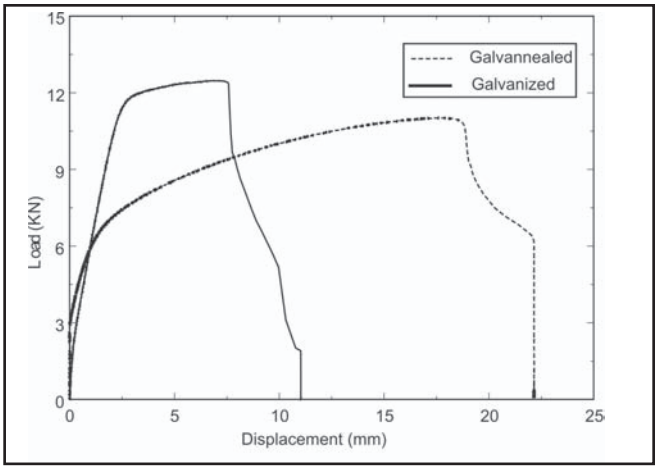

Fig. 2 — Load vs. displacement for spot welded specimens.

ducted to find the nugget diameter with respect to the major welding parameters as follows: welding current, electrode force, and welding time. The welding parameters were entered into an ENTRON controller and monitored with a DENGENSHA Ltd. WS-80 weldscope. With previous trials, fixed welding parameters were selected throughout the welding for a desired welding nugget diameter.

Two materials, a galvanized sheet metal and an automotive galvannealed sheet steel (1.6 mm thick), were used to make the tensile-shear spot welded specimens. Two strips of sheet steel were welded together in the center with a single electrical resistance spot weld, using the welding conditions listed in Table 1. Periodic peel tests were conducted during the specimen manufacturing, resulting in average nominal nugget diameters of 6.8 mm for the galvanized steel and 7.0 mm for the galvannealed steel sheet. The uniaxial load-displacement curve of the welded specimen at quasi-static loading condition is shown in Fig. 2, and a typical welded specimen shape and loading direction are shown in Fig. 1.

Experimental Procedure

Fatigue testing was conducted on an MTS 810 loading frame at a sinusoidal cyclic loading frequency of 5 Hz. Fatigue failure was defined as either a 30% drop of the load amplitude or more than 12.7 mm of deformation of the specimen in the loading direction. The fatigue test matrix is shown in Table 2, and a total of 15 nominally identical specimens were used to investigate the fatigue crack initiation and propagation process. The experimental results of the load amplitude (S_a) and fatigue failure cycles (N_f) relation are shown in Fig. 3.

The x-ray imaging was conducted on an AXR M130NH Minishot Cabinet X-ray machine. Figure 1 schematically shows the experiment setup. The x-ray accuracy was determined by a series of trials, and a benchmark "scratch" of 0.05 mm in depth and 0.1 mm in width could be detected clearly. The x-ray exposure condition was 120 kV at 12 min throughout this experiment, and the images were made using Kodak Industrex MX125 film. Multiple x-ray images of each specimen were taken at various percentages of the anticipated fatigue life.

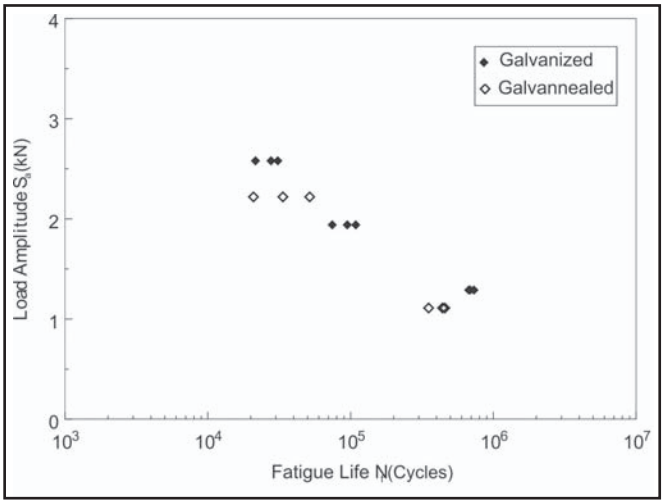

Fig. 3 — Load amplitude vs. fatigue life (S_a-N_f) curve.

Crack Initiation Location

Fatigue Experimental Results

The x-ray images indicated that the fatigue cracks did not always initiate from the notch root. In order to verify the crack location with x-ray images, a specimen was x-ray imaged, as shown in Fig. 4A, after nearly 70% of its fatigue life, and then cut through the center of the specimen in the loading direction. The cutting surface was polished, and an optical picture was taken as shown in Fig. 4B. These two pictures show that the crack initiates very close to the notch root, grows from inside of the two sheets to the outside of the surface in the thickness direction, and then propagates around the nugget in the width direction. The crack location and nugget shape of the spot weld are shown very clearly on the x-ray image. Figure 5 shows an etched spot weld section from another specimen, in which the boundary of the heat-affected zone can be seen with careful examination.

Figure 6 shows the crack initiation location distribution for various fatigue crack propagating modes (discussed subsequently). The crack location distance was measured along the central line in the loading direction. These measurements from x-ray images were taken early in the fatigue life of the specimen to minimize errors due to specimen distortion at the later stages of the fatigue life. Most of the cracks were located 0.2–0.8 mm from the nugget notch root edge.

Analysis of Crack Initiation Location

Due to the characteristics of the spot welding process, the intersection of the two welded sheets and nugget edge is often treated as a notch. Pan et al. (Ref. 9)

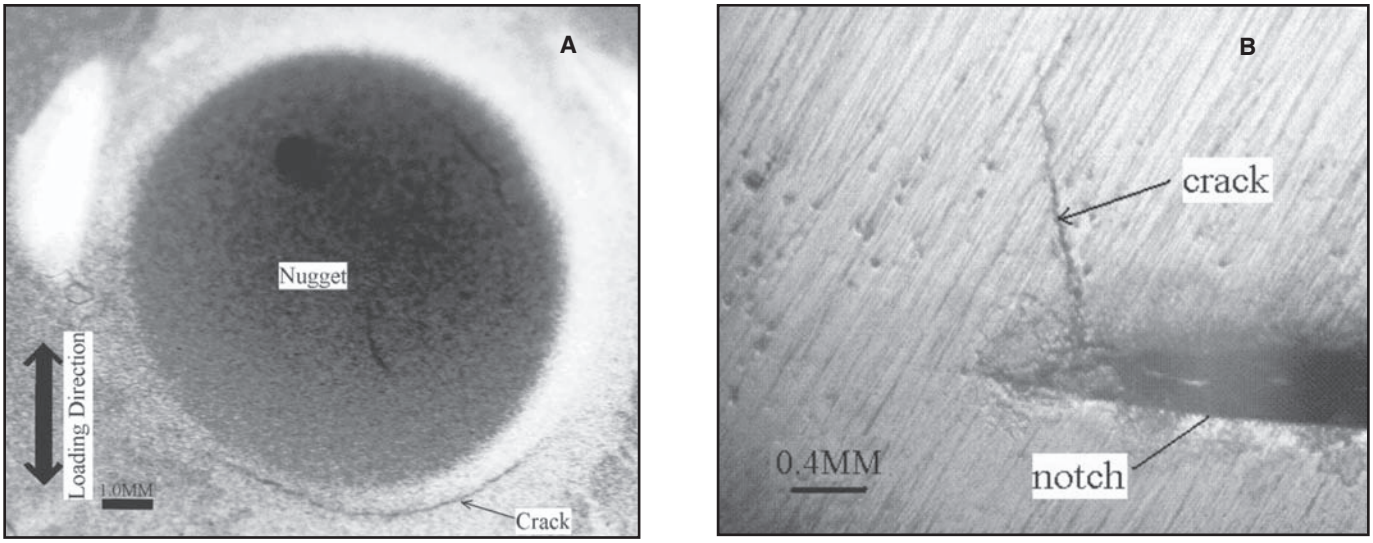

Fig. 4 — Crack location near the nugget notch. A — X-ray image; B — optical picture.

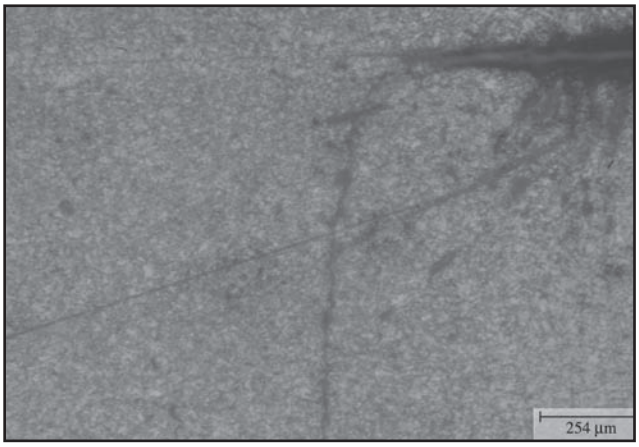

Fig. 5 — Etched (5% Nital, 2s) spot weld section with crack, 100X.

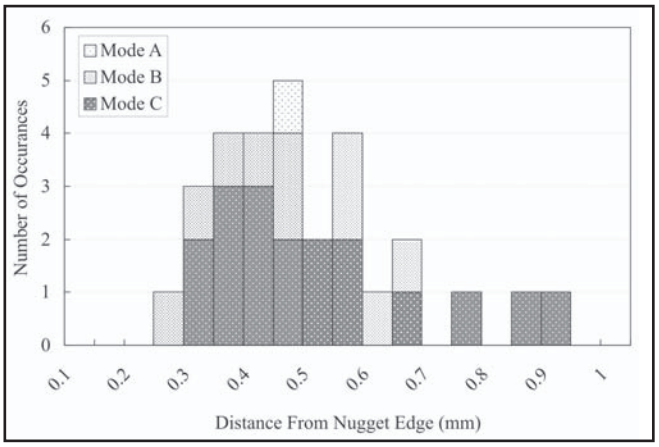

Fig. 6 — Crack initiation location distribution.

and Zuniga et al. (Ref. 10) treated this notch as a finite radius of 0.076 mm, and Radaj et al. (Ref. 11) suggested the maximum radius of 0.25 mm can be reached. The small radius of curvature is associated with a slight gap between the steel sheets of the lap joint. The existence of this gap is one of the reasons that the crack does not always initiate precisely at the nugget edge. Other factors are the different mechanical properties or stiffness of nugget area, heat-affected zone, and sheet material. In order to investigate the crack initiation location, both finite element simulations and theoretical analyses were conducted.

FEA Analysis

The ABAQUS finite element program was used to conduct the FEA modeling and analysis. The submodeling technique, which utilizes the direct interpolation technique to obtain the boundary values of submodel from global model, has been used to obtain the convergent results. The principles and applications of the submodeling technique can be found in Ref. 12. Half-symmetric models were created because of the symmetry of loading and structure, and 3-D, 20 node elements were used. The minimum element size for the final submodel was about 0.01 mm.

A series of finite element models were conducted to investigate the gap effect of the two sheets. The notch at the nugget edge was assumed as a semicircle, and the diameters studied were 0.08, 0.12, 0.16, 0.20, and 0.25 mm. Figure 7 shows the two typical von Mises stress distributions along the loading direction away from the nugget edge, and Fig. 8 shows the maximum von Mises stress location for the aforementioned gap distances. The maximum von Mises stress does not occur at the root of notch or nugget edge for any of these gaps. When the gap of two sheets increases, the maximum stress shifts away from the nugget edge. The distance of maximum stress from the nugget edge is about 0.1–0.2 mm for the gap distances that were modeled.

Theoretical Analysis

Creager et al. (Ref. 13) used the crack tip stress intensity factors to obtain the elastic stress distribution at the tip of deep slender notch for different loading modes. For Mode II, which can be applied to the tensile-shear spot welded specimen, the local notch stress distribution in the x-axis direction can be expressed as follows:

$$\sigma_{xx} = \frac{K_{II}}{\sqrt{2\pi r}} \frac{\rho}{2r} \sin\frac{3\theta}{2} - \frac{K_{II}}{\sqrt{2\pi r}} \sin\frac{\theta}{2}\left(2 + \cos\frac{\theta}{2}\cos\frac{3\theta}{2}\right) \quad (1)$$

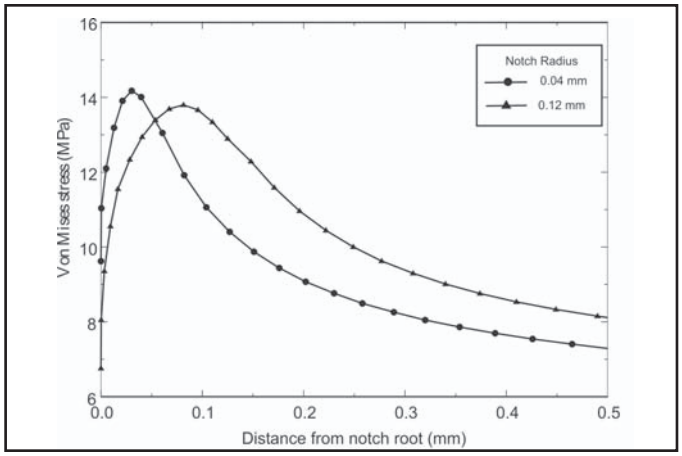

Fig. 7 — Typical von Mises stress distribution along the length (loading) direction.

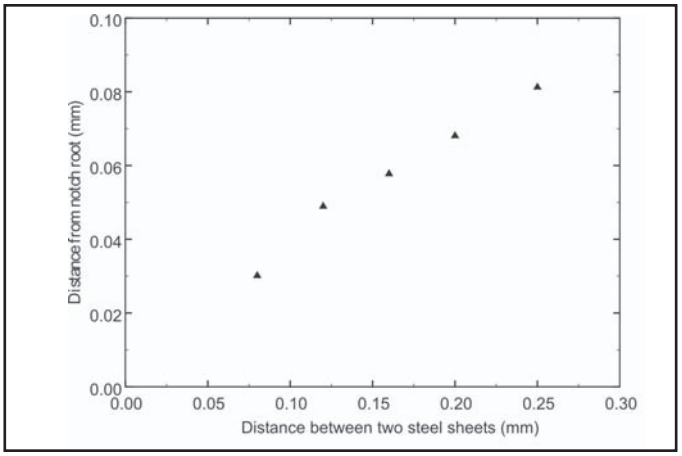

Fig. 8 — Maximum von Mises distribution along the length (loading) direction.

where K_{II} is the Mode II stress intensity factor, ρ is the notch root radius, and the definitions of r, θ can be found in Fig. 9.

If the shape of the notch root is assumed to be parabola, as shown in Fig. 9, on the interior surface, r, ρ, and θ have the following relation:

$$r = \frac{\rho}{1+\cos\theta}.$$

The Mode II stress intensify factor (Ref. 14) can be written as follows:

$$K_{II} = -\frac{p}{2sw\sqrt{2t}}$$

where s is the constant to consider the effective area of the nugget, p is remotely applied loading, and w and t are the width and thickness of sheet metal, respectively. The longitudinal stress σ_{xx} on the interior surface is as follows:

$$\sigma_{xx} = \frac{p}{4sw\sqrt{2\pi\rho\ t}}(1-\cos\theta)\sqrt{1-\cos^2\theta}. \quad (2)$$

With the relation above, the maximum value of longitudinal stress on the interior surface is at the angle (θ) of 120 deg or distance from the notch root is 2ρ. As stated previously, the notch radius can be 0.076–0.25 mm or the maximum stress will be occurring at 0.15–0.5 mm from the nugget edge. This data range is consistent with the experimental results shown in Fig. 6.

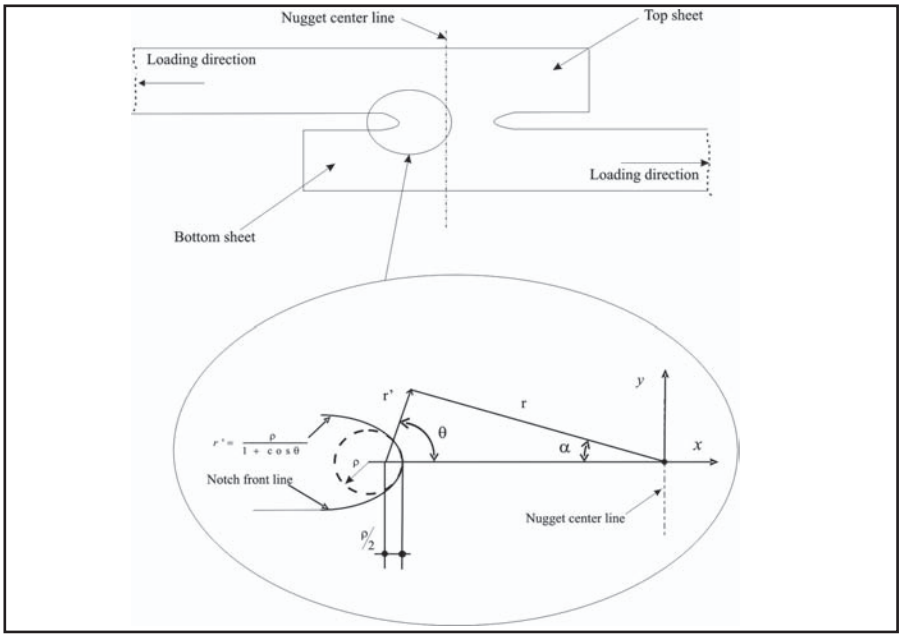

Fig. 9 — Deep slender notch with conic section (parabola).

Fatigue Crack Propagation and Modes

Fatigue Crack Propagation

The typical fatigue crack propagating process can be seen in Figs. 10–12. The cracks are initially on the inside of the specimen and cannot be seen directly before they propagate through the thickness of the steel sheet. The x-ray images among Figs. 10–12 show those interior cracks. The cracks usually initiated at opposite sides of the nugget, and crack propagation planes were perpendicular to the loading direction. Among the 15 specimens, one specimen exhibited two distinct cracks on one side of the nugget, while the other side only had one crack. All of the remaining specimens had only one crack on each side of the nugget. In general, a crack was initially observed on only one side. However, once a crack forms on the surface of the other side, it grows rapidly after initiation, especially near the end of the fatigue life of the specimen.

Fatigue Crack Propagating Modes

The fatigue crack propagation process can often be explained from knowledge of the local stress distribution characteristics. Three kinds of fatigue crack propagating modes were found in this fatigue experiment, as shown in Figs. 10–12.

In Mode *A* of Fig. 10, the fatigue crack initiated away from the nugget and propagated in the base steel sheet. The fatigue

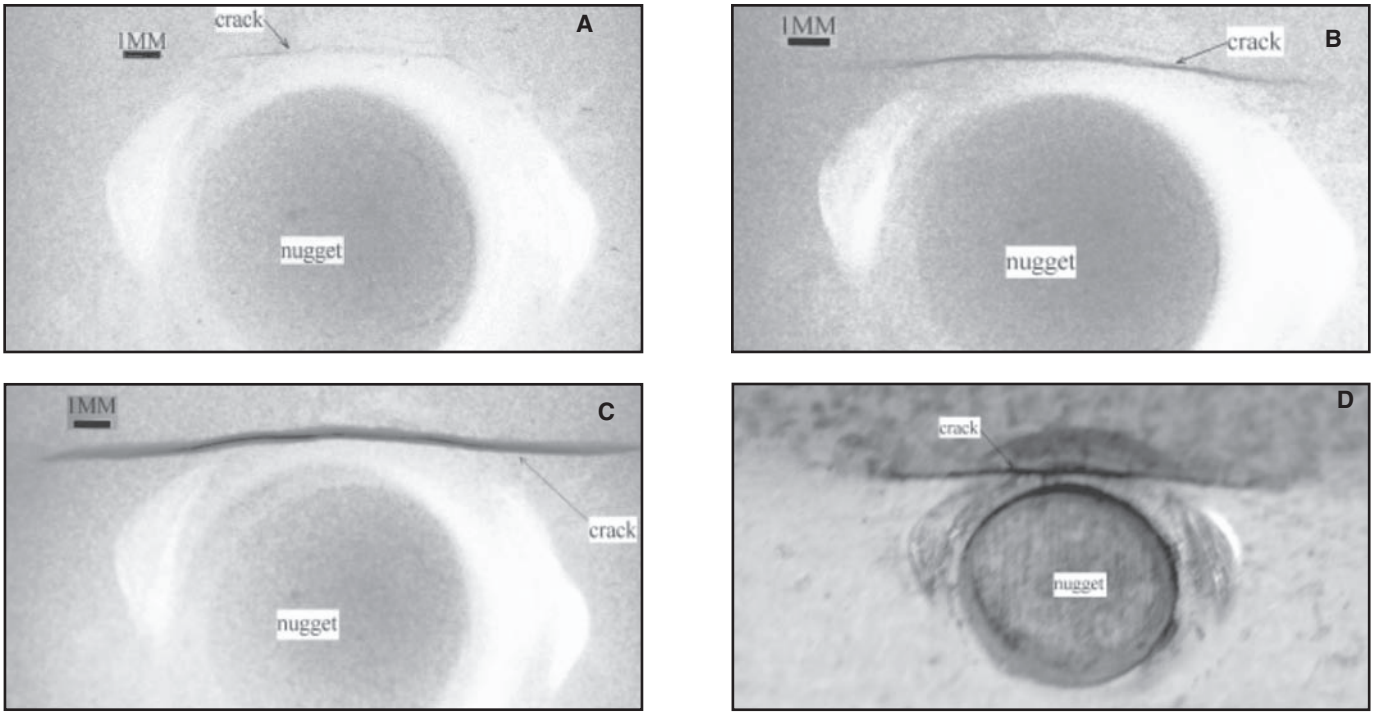

Fig. 10 — Fatigue crack propagating process — Mode A. A, B, and C — X-ray images; D — photo.

Table 1 — Spot Welding Conditions of Specimens

Spot Welding Parameters	Galvanized	Galvannealed	Units
Welding Current	10.9 ~ 11.0	9.9 ~ 10.0	kA[I]
Weld Time	22	22	Cycles[II]
Electrode Closing Force	4.5 ~ 4.7	3.9 ~ 4.1	kN
Electrode Tip Diameter	6.6	6.6	mm
Nominal Nugget Diameter	6.8	7.0	mm

I: Measured by a weldscope during welding.
II: 60 cycles = 1 second.

Table 2 — Fatigue Test Matrix and Life

Series #	Load Amplitude S_a (kN)	R-ratio	Fatigue Life N_f (Cycles)
GZ-A-1	1.29	0.05	730382
GZ-A-2	1.29	0.2	687785
GZ-A-3	1.29	0.3	672080
GZ-B-1	1.94	0.05	108753
GZ-B-2	1.94	0.2	94698
GZ-B-3	1.94	0.3	74362
GZ-C-1	2.58	0.05	27713
GZ-C-2	2.58	0.2	30936
GZ-C-3	2.58	0.3	21562
GA-A-1	1.11	0.05	352278
GA-A-2	1.11	0.2	457816
GA-A-3	1.11	0.3	440428
GA-B-1	2.22	0.05	20873
GA-B-2	2.22	0.2	33569
GA-B-3	2.22	0.3	51738

Notes: GZ — Galvanized steel; GA — Galvannealed steel.

Table 3 — Summary of Experimental Results from Mode, Fatigue Life Range, and Cracks

Mode	Galvanized Fatigue Life Range	Galvanized Cracks	Galvannealed Fatigue Life Range	Galvannealed Cracks
A	>700,000	1	>500,000	0
B	100,000 ~ 800,000	6	300,000 ~ 500,000	5
C	<100,000	11	<300,000	7

crack grew in a straight-line direction. The fatigue failure with this crack, as shown in Fig. 10D, is characterized by the specimen being broken into two parts. The failure crack plane is across the base steel sheet. This propagating mode of the fatigue crack usually occurs at low cyclic load levels or high cycle fatigue life regimes. Another important characteristic of Mode *A* is that the nugget does not rotate significantly. There were two cracks in Mode *A* for all experimental specimens.

Fatigue cracks in Mode *B*, shown in Fig. 11, usually initiated near the heat-affected zone and initially propagate around the nugget outline. Before it grows to approximately one-half of the nugget perimeter, the crack propagates in the base steel sheet until the specimen is broken. The nugget exhibits some rotation before the specimen is broken. The final failure shape with this fatigue crack mode is such that the weld partly breaks around the nugget edge and partly peels out the base steel sheet, as shown in Fig. 11D.

Figure 12 shows the Mode *C* of the fatigue crack propagating process. The fatigue crack will propagate along the perimeter of the nugget until it reaches the midline of the nugget. The final failure shape of this mode is that nearly half of the nugget peels off of each sheet, as shown in Fig. 12D. In this mode, the nugget rotates substantially to almost 90 deg.

The experimental results show that Mode *A* usually occurs at the low loading or high cycle fatigue process, the Mode *C* is usually under the high loading or low

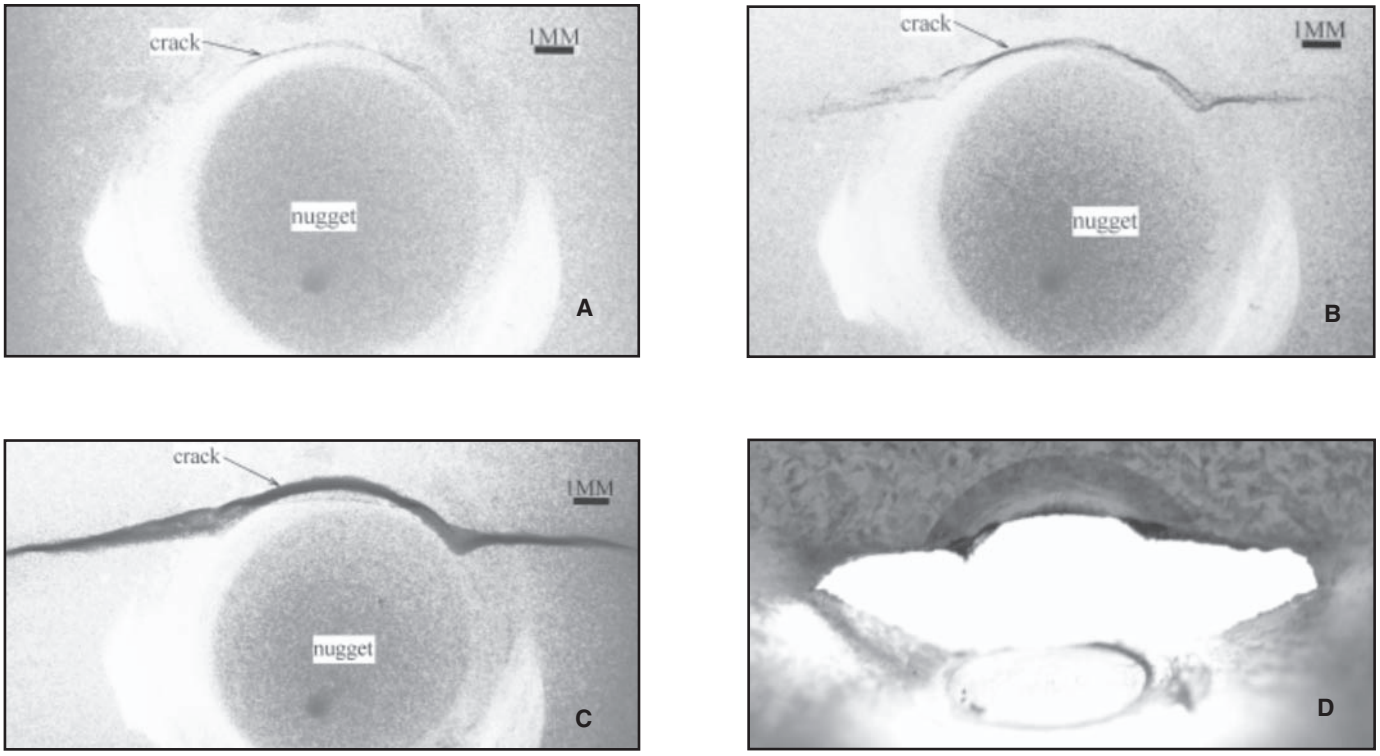

Fig. 11 — Fatigue crack propagating process — Mode B. A, B, and C — X-ray images; D — photo.

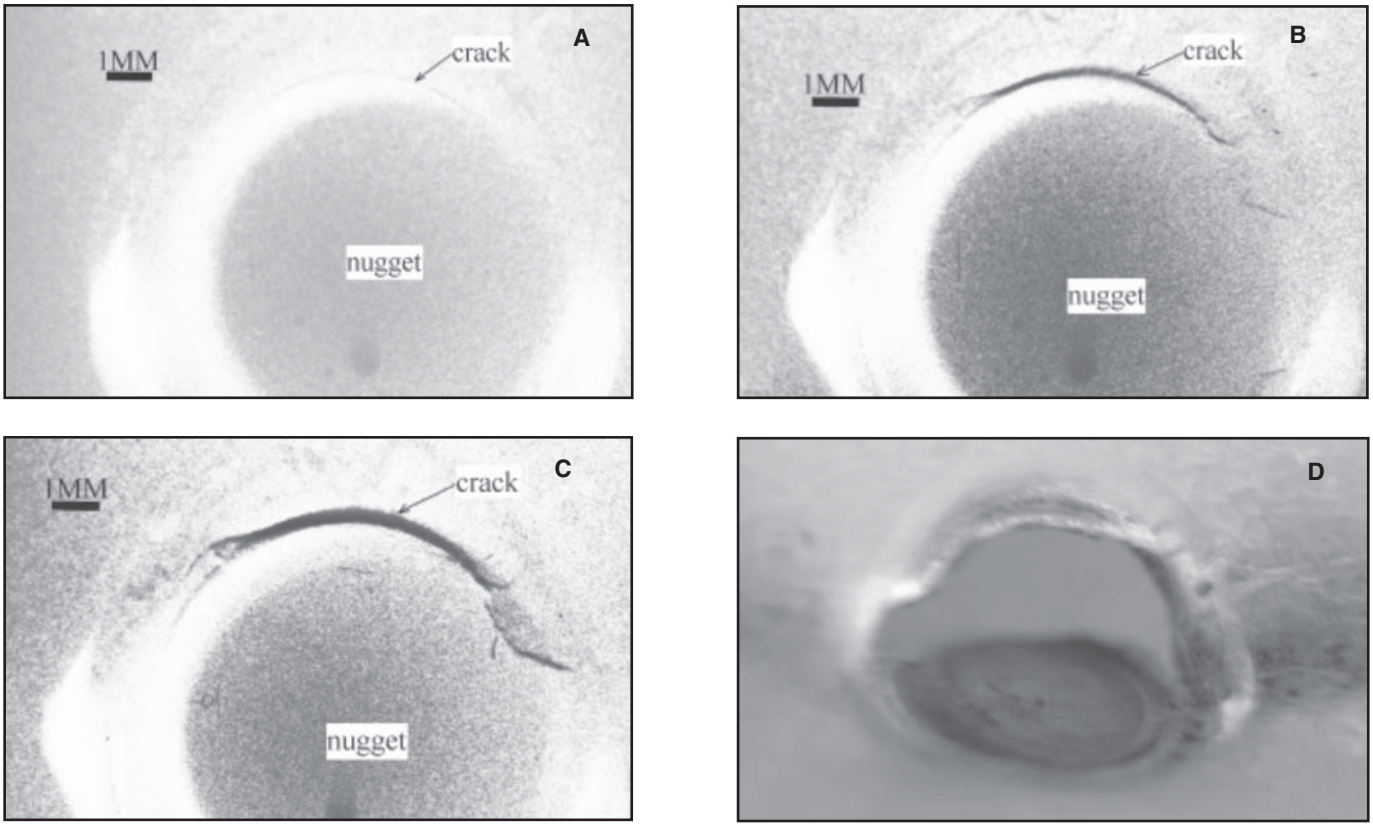

Fig. 12 — Fatigue crack propagating process — Mode C. A, B, and C — X-ray images; D — photo.

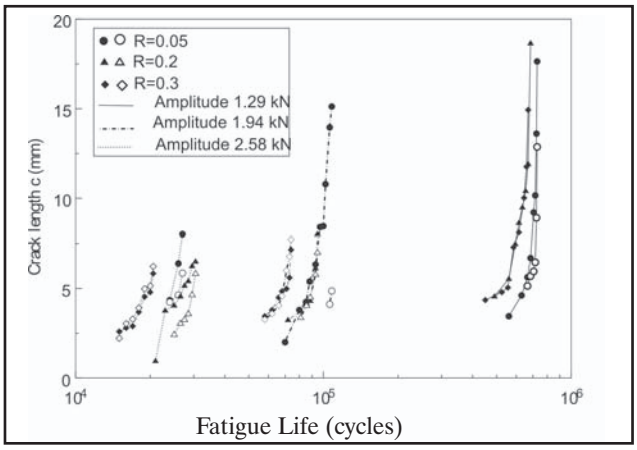

Fig. 13 — Crack length vs. loading cycles (metal: galvanized).

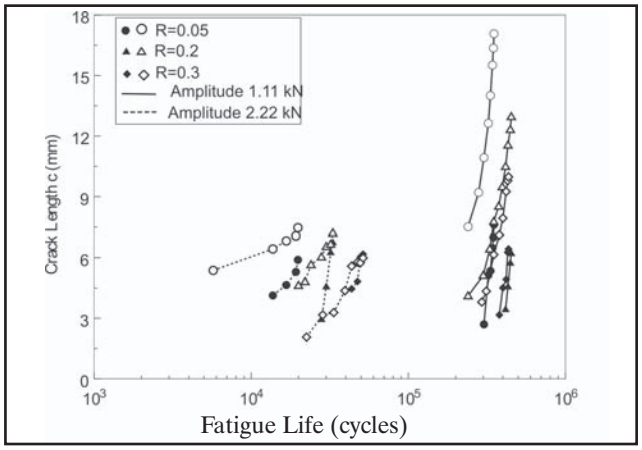

Fig. 14 — Crack length vs. loading cycles (metal: galvannealed).

cycle fatigue process, and the Mode *B* is between these two. Table 3 summarizes the relation of fatigue life and failure mode in this experiment. Among all of the experimental specimens, only two cracks propagated in Mode *A*, and most of the cracks are in Mode *C*. Another different characteristic of these three modes is that, on each side of nugget, the crack initiation and propagation rates were very similar during the fatigue cyclic loading in Mode *C,* and there is a very obvious difference from the other two modes.

One of the reasons for the different fatigue crack propagating modes is dependent on the different loading amplitudes. With high loading, due to the noncontinuous structure or high local stress concentration at the nugget root notch (Refs. 15, 16), the nugget area has rotated even at the beginning of fatigue cyclic loading. Such different rotations obviously have altered the local distribution of stress.

Crack Propagation and Fatigue Life Results

Figure 13 shows the crack length vs. fatigue life data for three different loading levels with galvanized sheet metal, and Fig. 14 shows the same relation for galvannealed sheet metal with two different loading levels. Usually there are at least two cracks separately initiating on the two sides of the nugget. The different sides are shown as solid and empty symbols on the aforementioned figures. Usually, one of the cracks propagates faster than another one, and the first observable crack initiated around 50 ~ 60% of the total life of the specimen.

Summary and Conclusions

The x-ray imaging technique has been used to investigate the fatigue failure process of tensile-shear spot welded specimens. The fatigue crack initiation location and propagation process were directly observed without damaging the specimens. Finite element results and results from an analytical model were presented that show the crack initiation location may not always occur at the notch root. These results lead to the following conclusions:

1. Experimental results show that the x-ray imaging technique is a very effective nondestructive examination method for observing the fatigue failure process of spot welded specimens, and the fatigue crack geometry and initiating location can be directly measured from x-ray imaged results.

2. Three typical fatigue crack propagating modes have been observed for experimental tensile-shear spot welded joints as follows: For low loading amplitude or high cycle fatigue failure, the crack can initiate away from the nugget and propagate in a straight line in base steel sheet, and for high loading amplitude or low cycle fatigue failure, the crack initiated near the nugget notch root and propagated around the nugget until reaching the middle of the nugget. Between these two, the crack initiated near the nugget root and then propagated into the base steel sheet.

3. The experimental results show that fatigue crack initiation locations are about 0.2–1.0 mm away from the nugget edge. Both the theoretical and finite element analyses show that the maximum stress location will not always be at the notch root of the nugget.

References

1. Pollard, B. 1982. Fatigue strength of spot welds in titanium-bearing HSLA steels. *SAE Technical Report No. 820284*, Detroit, Mich.

2. Davidson, J. A., and Jr. Imhof, E. J. 1983. A fracture-mechanics and system-stiffness approach to fatigue performance of spot-welded sheet steels. *SAE Technical Report No. 830034*, Detroit, Mich.

3. Barkey, M. E., Kang, H., and Lee, Y. -L. 2001. Failure modes of single resistance spot welded joints subjected to combined fatigue loading. *International Journal of Materials & Product Technology* 16(6-7): 510–527.

4. McMahon, J. C., Smith, G. A., and Lawrence, F. V. 1990. Fatigue crack initiation and growth in tensile-shear spot weldments. *Fatigue and Fracture Testing of Weldments, ASTM* Special Technical Publication, No. 1058, 47–77.

5. Cooper, J. F., and Smith, R. A. 1985. The measurement of fatigue cracks at spot welds. *International Journal of Fatigue* 7(3): 137–140.

6. Wang, G., and Barkey, M. E. 2004. Fatigue crack and its influence on the dynamic response characteristics of spot welded specimens. *Experimental Mechanics* 44(5): 512–521.

7. Wang, G., and Barkey, M. E. 2005. Fatigue crack identification in tensile-shear spot welded joints by dynamic response characteristics. *ASME, Journal of Engineering Materials and Technology* 127: 310–317.

8. Satoh, T., Abe, H., Nishikawa, K., and Morita, M. 1991. On three-dimensional elastic-plastic stress analysis of spot-welded joint under tensile shear load. *Transactions of the Japan Welding Society* 22(1): 46–51.

9. Pan, N., and Sheppard, S. 2002. Spot welds fatigue life estimation with cyclic strain range. *International Journal of Fatigue* 24: 519–528.

10. Zuniga, S. M., and Sheppard, S. M. 1995. Determining the constitutive properties of the heat-affected zone in a resistance spot. *Weld. Modeling Simul. Mater. Sci. Eng.*: 391–416.

11. Radaj, D. 1989. Stress singularity, notch stress and structural stress at spot-welded joints. *Eng Fract Mech* 134(2): 495–506.

12. ABAQUS User Manual, Version 6.4, Hibbitt, Karlsson & Sorensen, Inc. 2003.

13. Creager, M., and Paris, P. C. 1967. Elastic field equations for blunt cracks with reference to stress corrosion cracking. *International Journal of Fracture Mechanics* 3(4): 247–252.

14. Tada, H., Paris, P. C., and Irwin, G. R. 1985. *The Stress Analysis of Cracks Handbook,* Second Edition, Paris Productions Incorporated.

15. Deng, X., Chen, W., and Shi, G. 2000. Three-dimensional finite element analysis of the mechanical behavior of spot welds. *Finite Element in Analysis and Design* 35: 17–39.

16. Jr. Lawrence, F. V., Wang, P. C., and Corten, H. T. 1983. An empirical method for estimating the fatigue resistance of tensile-shear spot-welds. *SAE Technical Report No. 830035*, Detroit, Mich.